Impact of earthquake's epicenter distance on the failure of the embankment – A seismic prediction

Abdoullah Namdar
School of Civil Engineering, Iran University of Science and Technology (IUST), Narmak, Tehran, Iran

Omer Mughieda*
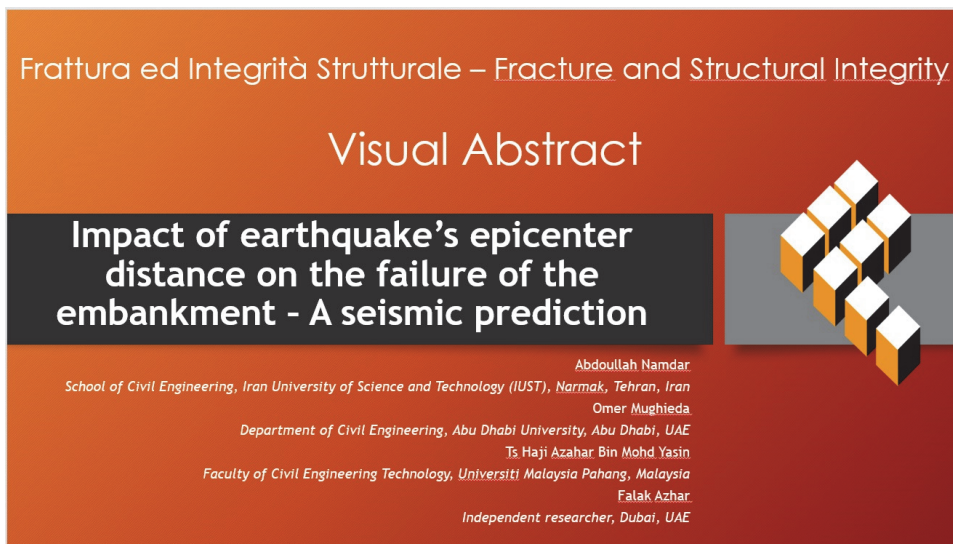*Department of Civil Engineering, Abu Dhabi University, Abu Dhabi, UAE*
omer.mughieda@adu.ac.ae

Ts Haji Azahar Bin Mohd Yasin
Faculty of Civil Engineering Technology, Universiti Malaysia Pahang, Malaysia

Falak Azhar
Independent researcher, Dubai, UAE

KEYWORDS. Embankment, Pre-existing Crack, Displacement, ANN, Damage prediction.

INTRODUCTION

Cracks in clay have undergone investigation through numerous experimental studies [1-3]. Rankine's theory and XFEM are generally applied to simulate cracks and predict the crack propagation angle and shape, respectively [4, 5]. One of the earlier observed experimental outcomes concluded that the angle of crack propagation in the clay is related to the brittleness of the clay [1]. In this regard, to validate the results of XFEM in crack propagation, the numerical simulation results [5] agreed with the experimental outcome [1]. Additionally, clay is used to build the embankment core due to its low permeability characteristics [6, 7], and by applying seismic acceleration to the ground, the crack in clay causes severe damage to the core of the embankment [8]. The impact of cracks on any embankment location requires thorough investigation. It is unclear whether the displacement's time and magnitude change with distance from the earthquake epicenter.

Seismic accelerations create nonlinear displacement on the embankment [9]. Various methodologies have been used to improve the stability of the embankment [10-14]. The stability of embankments can be increased with the use of several techniques, such as embankment fill, geosynthetic reinforcement, sheet piles and column installation, geogrid installation, and replacement fill [10-14]. Minimal research has been conducted on embankment distance from the earthquake epicenter for damage assessment of the embankment with the cracked core. However, some studies have analyzed pre-existing cracks on the embankment to apply feasible techniques for improving embankment stability.

The tension crack on the embankment usually occurs before applying seismic loading [15-18]. The top surface of the bentonite-sand mixture can crack due to shrinkage and desiccation [15]. Other reasons include erosion, swelling of soil [16], thaw settlement [17], and nonlinear volumetric deformation of soil in permafrost regions [18]. Pre-existing tension cracks extend with the application of seismic load. The geogrid and crushed-rock interlayers cannot prevent embankment cracking from the thaw settlement [17]. Therefore, it becomes necessary to simulate an embankment with pre-existing cracks for a smooth assessment of the seismic stability of the embankment.

Generally, a tension crack occurs in the crest of the embankment [8, 10, 19-22]. Several studies have concluded that pre-existing cracks on the embankment and earth structure reduce stability [23-26]. Field monitoring methods help classify embankment damage and the development of tensile cracks [27-30]. Numerical simulations and experimental work analyze the impact of the cracks on the instability of the embankment [31] and can assess crack propagation due to seismic acceleration [32]. Additionally, it is crucial to thoroughly investigate the differential displacement of embankment with pre-existing cracks related to the magnitude of seismic acceleration. During an earthquake, the seismic response of an embankment is related to the seismic acceleration's magnitude. Classifying earth structure damage as subjected to seismic acceleration from an earthquake is important.

In the present study, ANNs were used to predict displacement obtained by XFEM in association with the varying distances from the embankment model to the earthquake's epicenter. Additionally, the study has predicted how earthquake epicenter distance impacts the displacement's time and magnitude. These two essential parts of geotechnical engineering design have not been reported in the literature.

The objectives of this research work are;

- To assess applying the seismic acceleration of an earthquake with varying distances to the embankment model.
- To predict displacement in critical points of the embankment model.
- To study the time for the maximum negative and positive displacement occurrence.

MODELING AND SIMULATION

Damage in an earthquake-impacted area is not linear. Therefore, the factors that lead to damage need precise assessment. The earth structure's distance from the earthquake location must be studied to analyze the model's seismic response, and the numerical simulation needs to be investigated for the model's simulated earthquake response. The numerical simulation to explain this problem has the cost-effective, easy performance and quickly producing information advantage over the experimental simulation. The selected design parameters include the mechanical properties of the clay, sandstone, and recycled aggregate, the boundary condition of the model, and multidirectional applied seismic loading. In addition, according to theoretical concepts, clay is a non-tensile material. The simulated model has been subjected to seismic acceleration at different distances from the earthquake's epicenter. XFEM was used to produce ANNs with two hidden layers designed to predict the displacement based on the results. In order to validate the results of the numerical simulation, the outcome of the simulation has been compared to available data in the literature.

The geometry of the embankment impacts the model displacement [48]. As a matter of fact, when simulating problems with seismic waves, the edge effect can be present and should be taken into account in a complete model. However, in the present work, the influence of the model's dimensions is not taken into account for the sake of simplicity, although it is well-known that the geometric dimensions assumed for the foundation may affect the results. Fig. 1 is a demonstration of the model used in the numerical simulation. Part (a) is the simulated model, including the embankment and its foundation. The embankment is modeled from recycled material. The core and the foundation of the embankment are made of impermeable clay and sandstone, respectively. Parts (b) and (c) illustrate the model's boundary conditions, where the core of the embankment with cracks was simulated. In the seismic analysis of the model, the core embankment is critical, as the pre-existing crack of the model is located in the area. Fig. 1 part (d) graphically represents the application of seismic acceleration to each point at a model, where multi-directional seismic acceleration is applied to the model.

The lateral and vertical displacements on the embankment are linked to the soil's mechanical properties [9]. As this study considers the materials used to construct different embankment areas, it is necessary to analyze the displacement at the critical point of the model.

The vertical displacement that occurs at the embankment's crest reduces the seismic safety of the embankment [28]. In the current study, points located in the crest and center of the embankment's slope have been considered for investigation of the seismic vertical displacement.
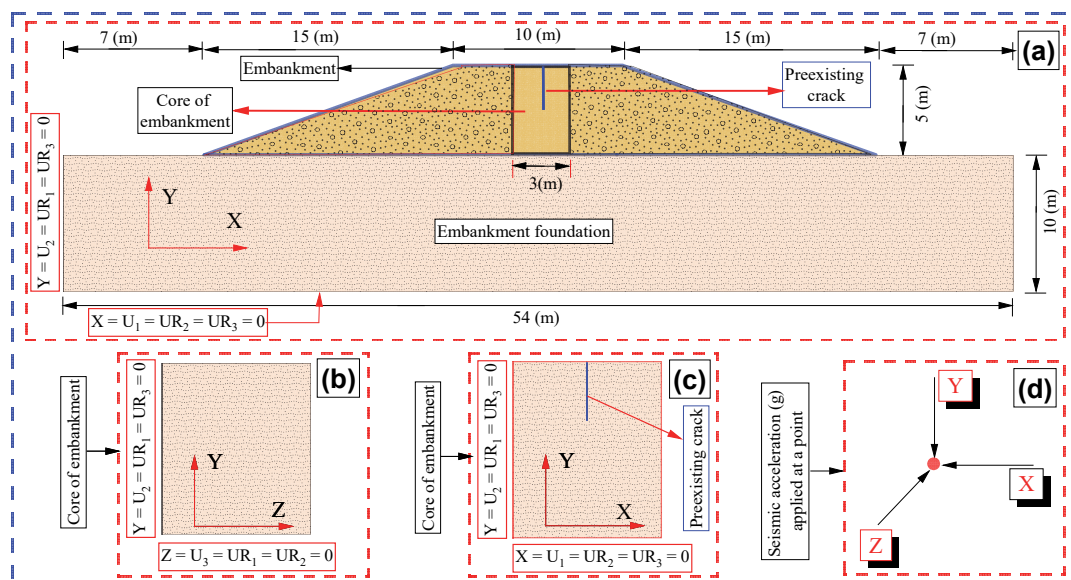

Figure 1: Model and boundary conditions, a) simulation of the embankment and its foundation models, b) core of the embankment at Y-Z plane, c) core of the embankment at Y-X plane, d) the application of seismic acceleration to each point of the model.

Material	Friction angle, ϕ (deg)	Cohesion, C_u (kPa)	Poisson's ratio, ν	Unit weight, γ (kN/m³)	Modulus elasticity, E (MPa)	Ref
Clay (Undrained)	-	25	0.3	18	12.5	[34]
Recycle aggregate	40.6	-	0.25	23.3	27620	[35]
Sandstone	-	-	0.25	24	35000	[36]

Table 1: Mechanical properties of clay, recycled material, and sandstone [34-36].

MECHANICAL PROPERTIES

I n the geo-structure seismic simulation, the type of the geomaterials impact the embankment's displacement. The material's location also influences the model's mechanical properties and displacement [33]. The embankment is made of two types of materials. Clay was used to build the embankment's core, and the recycled aggregate was used in other areas. A sandstone foundation was used for embankment installation.

Tab. 1 describes the mechanical properties of clay, recycled aggregate, and sandstone used in the simulation of the embankment and subsoil [34-36]. Clay limits water flow due to its impermeable nature [37]. The material is considered low in strength. Recycled aggregate can be utilized for embankment construction as it can provide acceptable seismic resistance to the embankment [33]. Compared to the embankment, the foundation behaves with the solidified part of the model.

SEISMIC DATA

On 21 March 2023, an earthquake with 5.6 MWW occurred in the Melipilla region of Chile. The earthquake's epicenter was measured at a depth of 65 (km) and coordinates of -33.6103 and -71.3517. Four different acceleration histories (registered at four different stations located at a distance of 24.9 (km), 38.3 (km), 65.9 (km), and 84.5 (km) from the epicenter of the earthquake) are here considered and used as input data in four different models. These histories are shown in Fig. 2. This numerical simulation aims to assess the impact of the epicenter distance on the seismic response of the embankment. The acceleration changes as it shifts farther from the earthquake epicenter. The multi-directional seismic acceleration must be applied to the model to improve the results' accuracy in the numerical simulation [39]. Fig. 1 depicts that appropriate modeling was done considering the nature of the seismic acceleration occurring in the field. The seismic acceleration of the earthquake with 5.6 MWW at 0°, 90°, and 360° has been applied to the model.
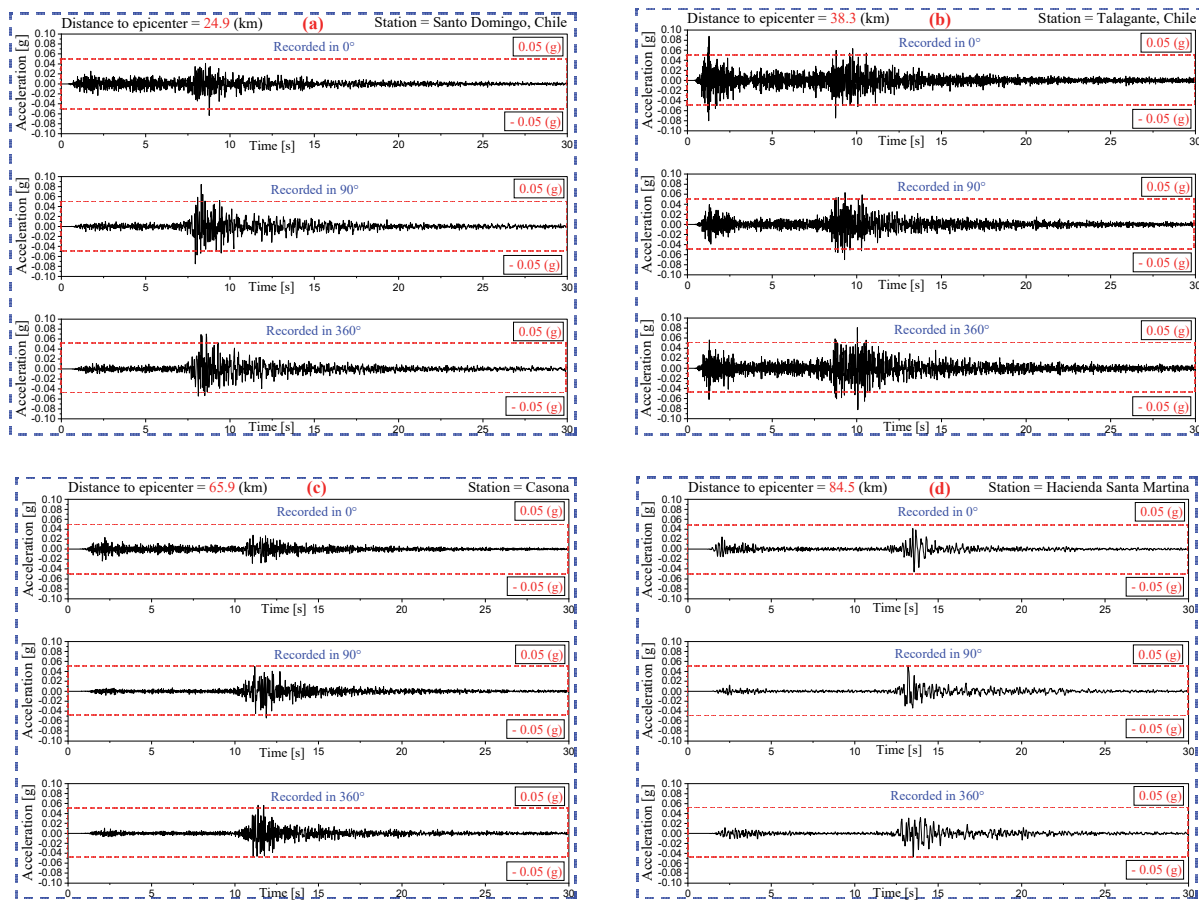

Figure 2: The acceleration history (g) for different distances from the epicenter

CRACK THEORETICAL CONCEPTS, SIMULATION IN FEM, AND REALITY

According to Rankine's theory (1857), the pre-existing cracks on clay are simulated [5], and crack propagation is predicted by using the XFEM [4]. The crack propagation angle in the brittle clay sample is higher than in the ductile clay sample [1]. This phenomenon was simulated and proved using the XFEM. It was observed that the clay with higher brittleness faces the crack propagation with a higher angle when subjected to seismic acceleration [4]. The failure

model of the clay model with pre-existing cracks is associated with the brittleness of the clay. Fig. 3 shows the type of crack that occurred on the Akitsu River embankment due to the Kumamoto earthquake in Japan in 2016 [8]. Based on theoretical concepts and evidence based on reports, Fig. 3 illustrates the embankment crack, which is simulated and presented in Fig. 1. This study simulated the single longitudinal pre-existing crack on the embankment. It assumed the location of the crack at the center of the embankment's crest. Simulation of the crack shape was followed by simulating the crack depth, which was calculated using Rankine's theory.

Using Rankine's theory for undrained clay, Eqns. 1 and 2 are applied to calculate the length of the pre-existing crack and identify the solid zone in the core of the embankment [40].

$$Z = \text{Length of the preexisting crack} = 2c_u \ / \ \gamma \tag{1}$$

$$S_z = \text{Solid zone} = H_0 - Z \tag{2}$$

Fig. 3 depicts the pre-existing crack on the clayey core of the embankment. It assumed the core of the embankment is under undrained conditions. The fully saturated undrained clay has ϕ_u equal to zero.
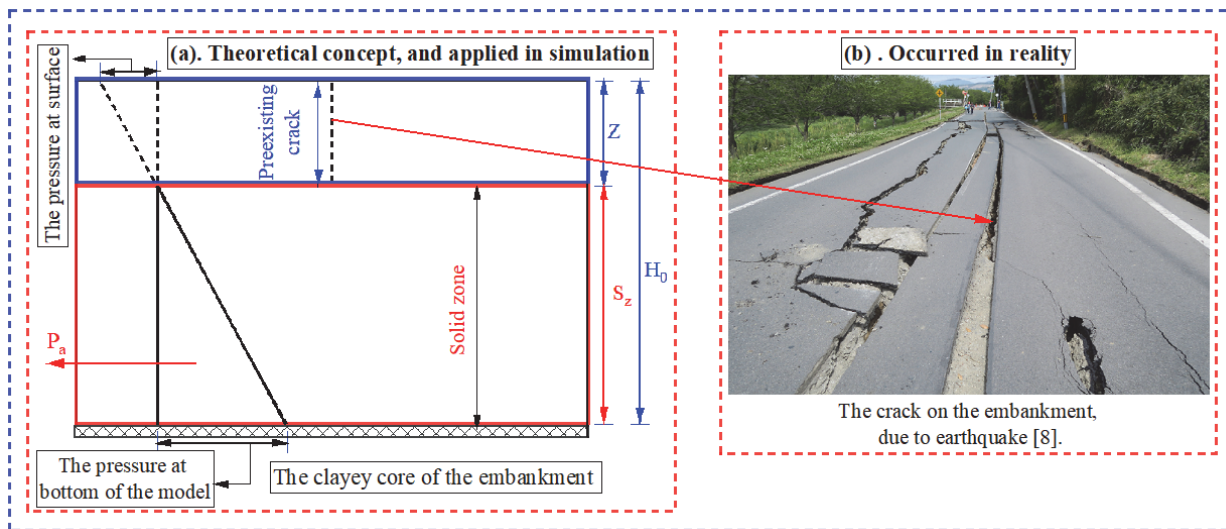

Figure 3: The preexisting crack on the clayey core of the embankment.

In a realistic crack simulation model, the crack orientation should be free to rotate. The model should comprehend that pre-existing crack and crack propagation behave differently. Furthermore, it should be able to identify tensile and shear failure [41]. XFEM is a feasible platform to simulate crack propagation to satisfy these requirements. Fig. 3 (b) shows a type of crack in case of two earthquakes occurring subsequently in a short time. The crack created in the first earthquake will be a pre-existing crack for the second earthquake.

Assuming the crack opening occurs parallel to the major principal tensile stress, the crack strain in this direction can be calculated [42], in addition, the finite elements were applied to crack growth [43-44].

A 2004 study proposed the phantom paired element approach for crack propagation, using node generation according to the material's properties [45]. The phantom node method describes the node generation in the crack opening and propagation. A later research study in 2016 used the ABAQUS to implement XFEM to simulate the crack opening and propagation process [46]. The current study used ABAQUS to perform the phantom node method to simulate crack opening and propagation. Fig. 4 depicts the function of the phantom node method for generating mesh in crack opening and propagation. Fig. 5 illustrates the simulated model using ABAQUS to perform the nonlinear numerical simulation. Nodes 192 and 1434 have been selected as critical points of the model. Evaluating the displacement in these two points helps with the model's stability analysis and prediction failure.

The number of nodes and elements for the models are 10212 and 8690 respectively. The type of the mesh is C3D8R. The mesh dimension for the model is 1350 mm. Due to the preexisting crack in the embankment model, the extended finite elements method was used in performing ABAQUS. Different parts of the embankment model interaction were modeled using the contact algorithm presented in ABAQUS by creating a tangential interface.
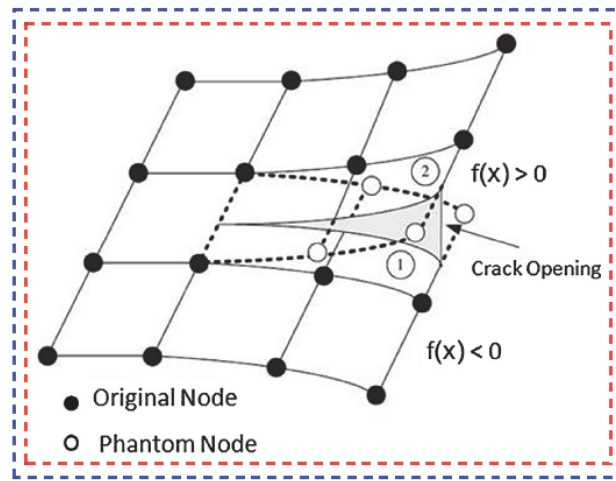
Figure 4: The phantom node method for generating mesh in crack opening and propagation [45].
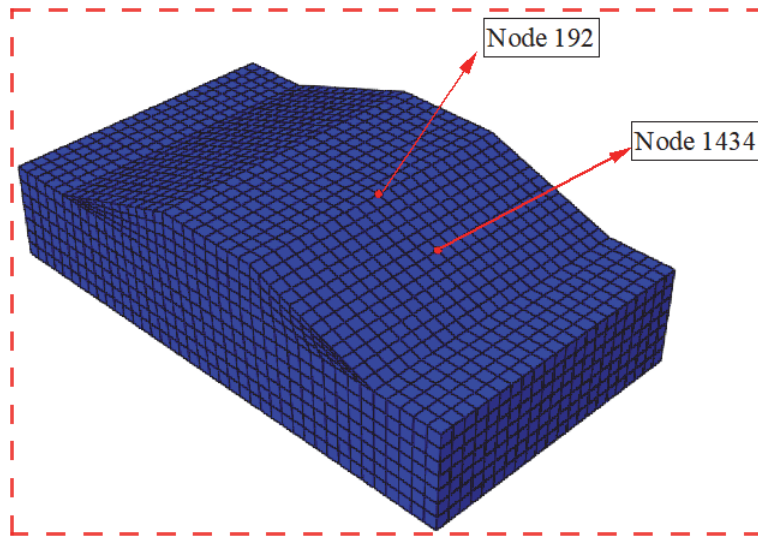

Figure 5: Model in the numerical simulation.

ARTIFICIAL NEURAL NETWORKS

Statistical analysis is usually preferred for predicting and classifying results in geotechnical engineering [33, 47-48]. Artificial neural networks (ANN) can significantly support geotechnical engineering designs as they can be used for the integration, prediction, and classification of results [49-52]. ANN is also commonly used for results of investigation forecasting, categorization outcome of a phenomenon study, association of data, and filtering interpreted data for solving several engineering problems [53-57]. An ANN is created from input, hidden, and output layers, with neurons performing at each layer [52]. In a recent 2020 study, ANN was proposed with two hidden layers with an architecture of 6:7:5:1 for the input layer, first hidden layer, second hidden layer, and output layer, respectively [58]. The multilayer perceptron (MLP) is a wholly associated class of feedforward ANN [59]. This study used the MLP method with the Levenberg-Marquardt algorithm to project the ANN for the classification and prediction of the displacement in a selected model point.

The following equations were used in ANN [60]:

$$f_j = \frac{2}{1+e^{-2Zj}} - 1 \tag{3}$$

$$Z_j = \sum_{i=1}^{n} W_{ij} x_i + b_j \tag{4}$$

$$f = \tanh\left(w_2 \times \left[\begin{array}{c} \tanh(W_1 \times X) \\ 1 \end{array}\right]\right) \tag{5}$$

$$X = \left[\overline{t}, \overline{l}_1, \overline{x}_1, \overline{y}_1, \overline{l}_2, \overline{x}_2, \overline{y}_2, \overline{l}_3, \overline{x}_3, \overline{y}_3, 1\right]^T \tag{6}$$

where;

f_j is output of jᵗʰ neuron

Z_j is data gathering of jᵗʰ neuron

x_i is input

w_{ij} is weigh

b_j is bias

w_1 is weight matrices linking the input and hidden layers

w_2 is weight matrices linking the hidden and output layers

X is the augmented input vector

In reference to the literature [61], Eqns. 7-8 are used to control prediction quality.

$$RMSE = \frac{1}{n} \sum_{i=1}^{n} \left(d - d_p\right)^2 \tag{7}$$

$$R^2 = 1 - \frac{\sum_{i=1}^{n} \Sigma \left(d - d_p\right)^2}{\sum_{i=1}^{n} \Sigma \left(d - \overline{D}_o\right)^2} \tag{8}$$

d is the obtained displacement by XFEM, d_p is the forecasted displacement by ANNs and $\overline{D}_o$ is the mean of displacement from FEM.

The quantity of neurons in the hidden layer design significantly affects the output accuracy of prediction and classification performed by the ANN model [62]. In this investigation, two hidden layers were selected for ANN.

RESULTS AND DISCUSSION

The earthquake's impact on embankment damage was numerically investigated by assessing displacement, stress, and strain in nodes 192 and 1434 of the model in the crest and middle of the embankment's slope. The results of the nonlinear numerical simulation revealed that the location of the embankment and its distance to the earthquake's epicenter is critical.

According to Fig. 6, with an increase in the distance of the embankment to the earthquake's epicenter, the time for the occurrence of the maximum negative and positive displacement in the selected points is nonlinear. The time and magnitude of the maximum displacement at each model are different. The maximum negative and positive displacements in the Y direction of nodes 192 and 1434 were observed at 24.9 kilometers from the earthquake's epicenter. Additionally, the measurements of displacement against distance from the epicenter can be observed to follow a nonlinear pattern. Model - 1, Model - 2, Model - 3, and Model - 4 are located at distances of 24.9 (km), 38.3 (km), 65.9 (km), and 84.5 (km) from the earthquake's epicenter, respectively.
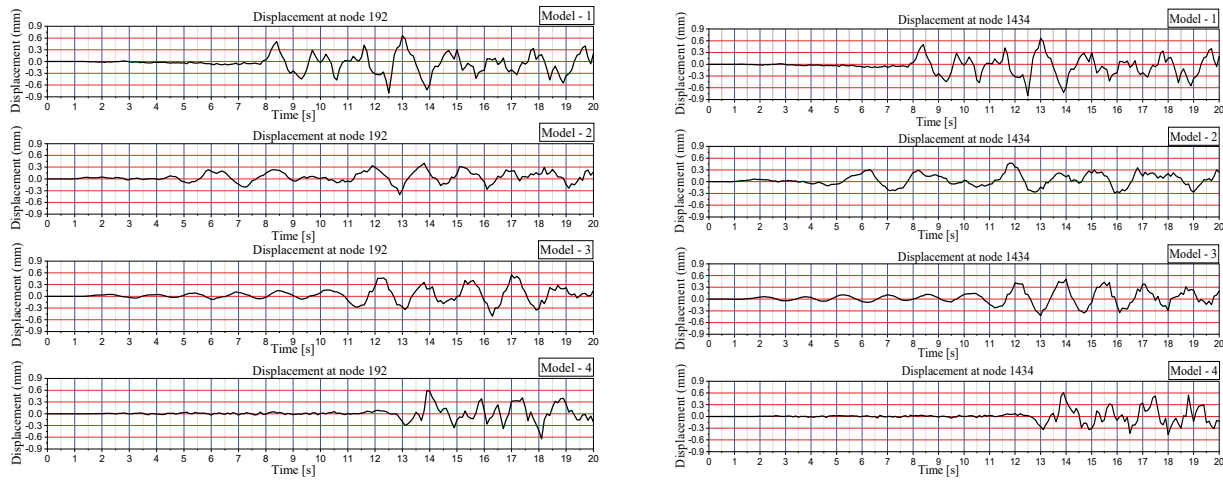
Figure 6: Displacement in models 1 - 4, at selected points

Vertical displacement occurs at the embankment's crest, and there is no seismic safety for the embankment when faced with unallowable displacement [28]. In the current study, node 192 is located in a critical part of the embankment and has been considered for investigation of the seismic vertical displacement in previous research work [14]. The slope movement accelerates the displacement of the crest [10], and nodes 192 and 1434 present the displacement of the crest and slope vertical movement. The displacement in node 192 differs from the displacement in node 1434 within all models.

Fig. 7 shows the maximum deformation against the first maximum multidirectional displacement in models 1– 4. In model 1, maximum multidirectional displacement occurs at 8.4 seconds, at a distance of 24.9 km from the earthquake's epicenter, while in models 2-4, the maximum displacement occurred at 5.8 seconds, 12.2 seconds, and 14 seconds, at distances of 38.3 km, 65.9 km, and 84.5 km from the earthquake's epicenter, respectively. The distance from the earthquake's epicenter mostly leads to a delay in maximum multidirectional displacement. Model 2 follows faster displacement and a higher deformation level than models 1, 3, and 4. The deformation based on the shear strain occurs at different times for each model.
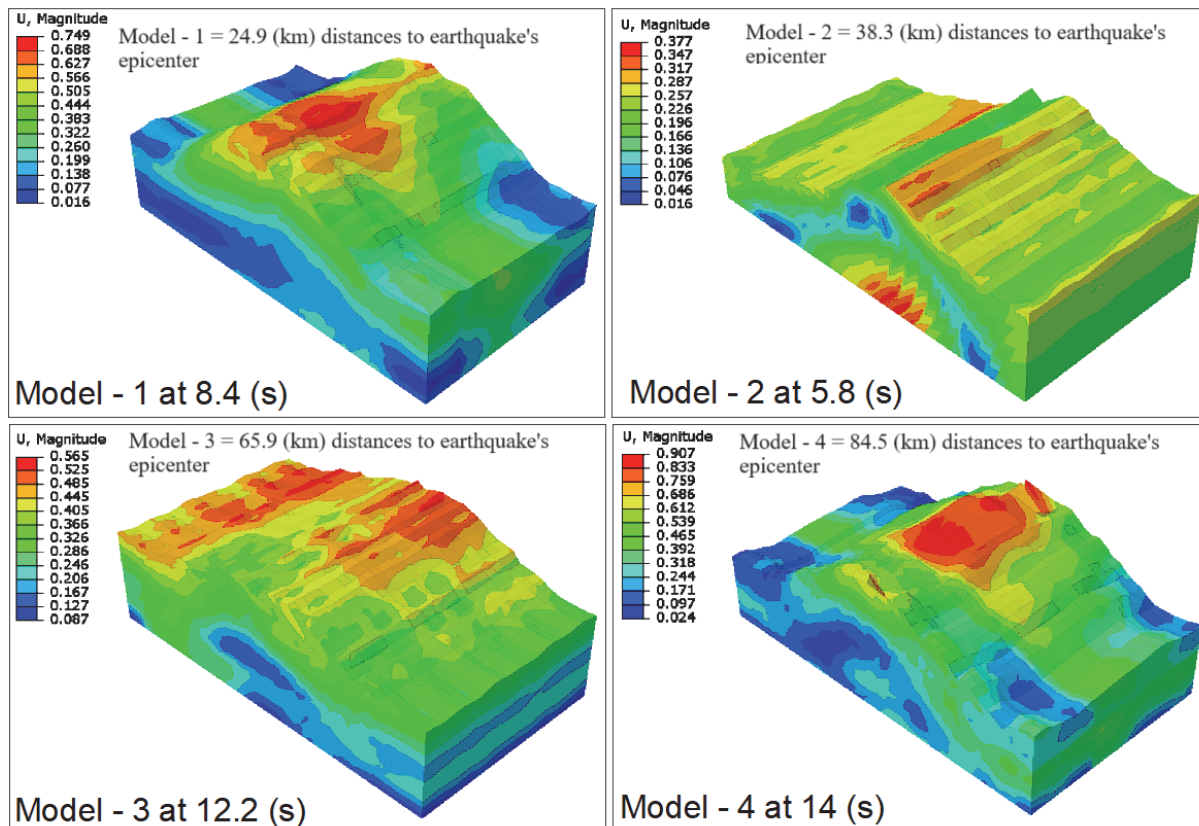

Figure 7: Maximum deformation against first maximum multidirectional displacement in models 1 – 4.

As part of a 2023-based study by Namdar et al., prediction of the cracked soil using XFEM was reported [5], and the type of crack was analyzed by considering crack propagation and mechanical properties of the material. The crack propagation angle is more prominent for a brittle material in comparison to a ductile material [1]. The crack will be propagated based on the mechanical properties of the material. The shape of the cracks and the possibility of crack propagation are associated with the mechanical properties of the materials [5]. In the present study, due to the nature of the seismic acceleration, mechanical properties of the soil, and geometry of different sections of the model constructed from the soil and recycled aggregate, the crack has not been propagated during the application of seismic load on the model. The lateral force from the slope of the embankment does not allow the crack propagation.

Figs. 8 and 9 show the fluctuation of maximum dynamic nonlinear deformation produced by stress and strain in nodes 192 and 1434 of models 1-4. The maximum intensity of the stress and strain is observed when the model is located at a 24.9 km distance from the earthquake's epicenter. The deformation speed changes as the model's location from the earthquake's epicenter changes. An increase in displacement of the model leads to faster deformation. By comparing all models, it can be observed that the distribution of the deformation is nonlinear. Maximum deformation for all models was observed in the crest. Vertical strain and stress values vary for each model at nodes 192 and 1434.

Tension cracks occur at the top of the embankment and not the bottom. When the embankment is subjected to seismic loading, the crest of the embankment fails due to tensile force, and the bottom part fails due to shear force [8]. Tensile failure precedes shear failure with low vertical stress. Due to this phenomenon, the crack will not be propagated in the embankment model when a preexisting crack during the embankment model is subjected to seismic acceleration. In this study, the crack has not been propagated from an initial condition of the model. The maximum intensity of the stress and strain is observed when the model is located at a 24.9 km distance from the earthquake's epicenter. The distance of the model plays an essential role in seismic stability. The stress-strain curve does not present shearing tensile in the model. When the compressive stress governs the model deformation, it does not cause crack propagation.
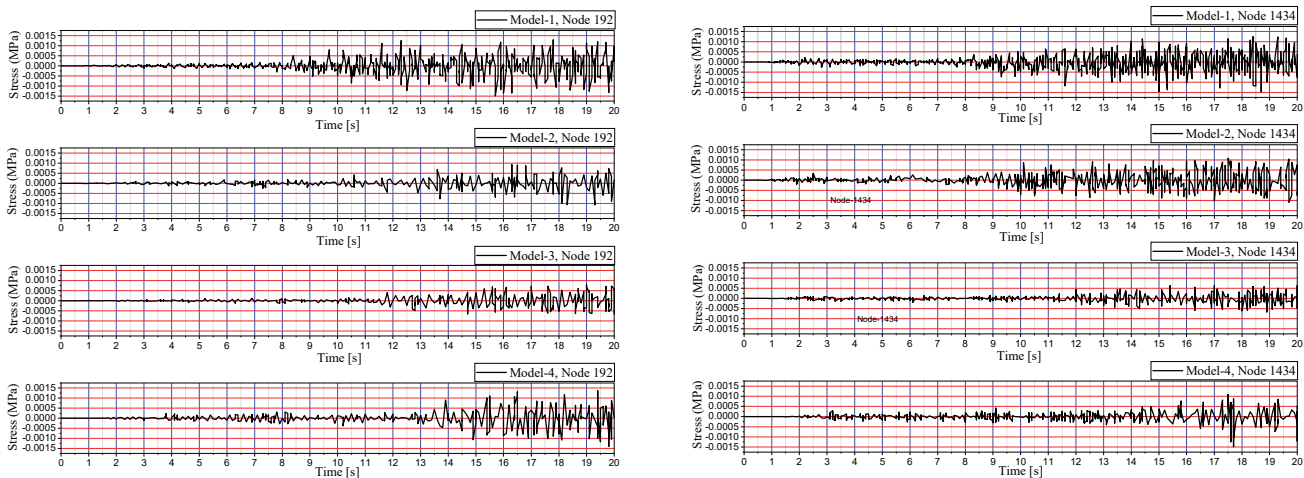

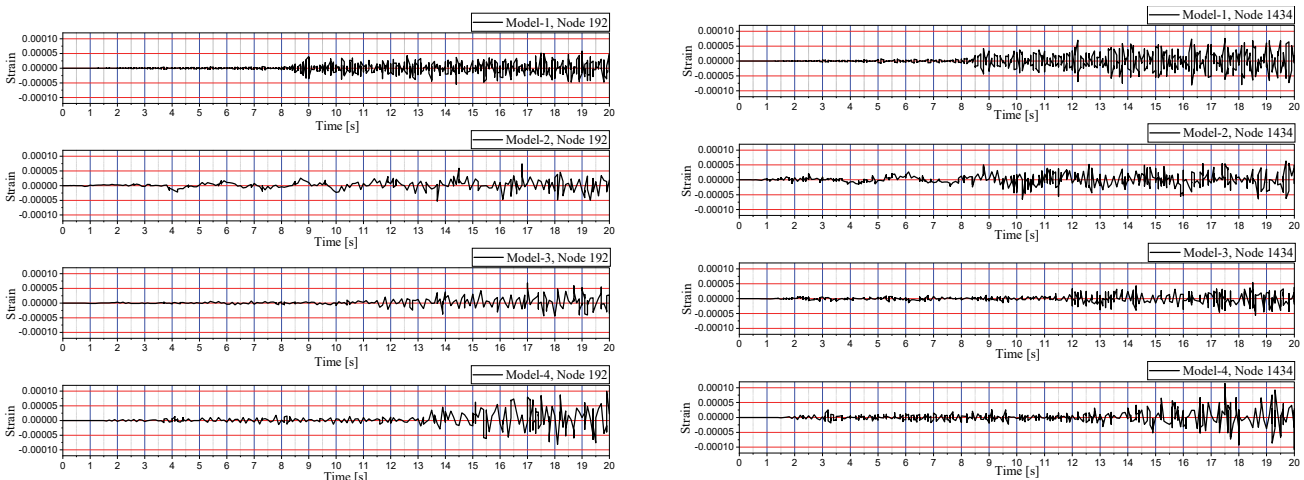Figure 8: Stress in models 1 – 4 at selected points.

Figure 9: Strain in models 1 - 4 at selected points.

A 1988 research study by Vallejo stated that the propagation angle of the secondary cracks in the ductile samples of clay is a function of the water content in the samples [1]. In addition, large tensile strains do not aid in the development of crack openings. In a model, tensile cracks occur when one of the principal stresses is tensile [31]. Therefore, the stress-strain relation is vital in crack opening and propagation. The preexisting crack minimizes the seismic stability of the embankment. The nature of the seismic acceleration interaction in developing tensile strain and stress in a location of the model causes crack propagation. Under compressive stress-strain conditions, the crack propagation was not observed in the numerical simulation.

As part of the conventional design, only the strength and magnitude of the ground motion are considered. The distance of the embankment to the earthquake's epicenter causing changes in the results is not taken into consideration. According to the present study, there is a need for the seismic embankment to assume different distances from the epicenter of the earthquake and integrate the results by applying ANN.

APPLICATION OF ARTIFICIAL NEURAL NETWORKS

As stated in the literature, in many cases, a tension crack occurs in the crest of the embankment [8, 10, 19 - 22]. As part of the current study, ANN has been applied to four models, and the displacement in the crest of the embankment has been assessed. The ANN has been designed with two hidden layers. The prediction accuracy needs to be improved due to the complex failure mechanism of the model. The parameters in ANN input are the vertical peak, strain, displacement, and times of peak occurrence. Using Abalone Data Analysis in performing Levenberg-Marquardt algorithms, 3927 data values in the data ring value were observed to predict displacement. The data in ANN is divided into training, testing, and validation. These three groups of data are representative of the sample population in the ANN. In applying ANN to geotechnical engineering data are randomly divided into three subsets: training, testing, and validation with different percentages. In the presented work data was subdivided to obtained data from XFEM, forecasting data, standard deviation, and mean data for all sets of the training, testing, and validation with different percentages. These data values are efficient and applicable to the prediction process. The ANN for the classification and prediction of the displacement in a selected model point.

Tabs. 2-5 present the data used in the ANN. Fig. 10 shows regression analysis for displacement prediction at the Y direction in models 1-4 at node 192. Data separation is divided into training, testing, and validation. The combination of all these parts is presented in a new figure. The testing set performs the ANN, and subsequently, the training is stopped by the validation set. The training process is crucial in finding regression results in an ANN model. The RMSE and regression value R indicate performance assessment of the ANN for comparison statistical analysis. It has been observed that the prediction of ANN for each model has a different quality according to the data quality provided by FEM. Accurate predictions using FEM results can be challenging.

In the adjustment of the model parameters, a training set will be employed. The testing set is used to control the quality function of the ANN model at different steps of training to avoid overfitting. In the organized ANN architectural design, the validation set is used to assess the function of the trained network [63]. The overfitting takes place when the data points in the training set are small [64]. In the present work, to perform the ANN based on Levenberg-Marquardt Algorithm, the Abalone Rings Data Set mode was used, and based on the selected technique 3927 data values were generated. The increasing number of data values supports avoiding overfitting.

By designing an accurate ANN, overfitting will be avoided, and an accurate relationship between input and output will be constructed [65–66]. In addition, overfitting may occur when the training error is smaller than the validation error [67]. The RMSE for all models is summarized in Tab. 6. There is no overfitting in models 1-4 during all phases of the ANNs. The overfitting represents an error in the networking.

The diagram of the cost function variations from RMSE has been revealed in Fig. 11. This cost function variations chart has been depicted for each model concerning the training, validation, and test data. Fig. 11 shows the prediction accuracy of displacement in the Y direction for models 1-4 at node 192. Tab. 6 presents R^2 and RMSE obtained for models 1-4 in the ANN. The regression value indicates that the displacement is well predicted. Based on the results of the ANN, the prediction outcomes are acceptable.

No	Time (s) of Peak Strain	Vertical Peak Strain	Time (s) of Peak Displacement	Vertical Peak Displacement (mm)
1	9	3.66158E-5	1.2	0.00353
2	9	3.66158E-5	2.8	0.01323
3	10.2	1.11211E-5	5.1	-0.0551
4	10.2	1.11211E-5	6.1	-0.08055
5	10.6	2.48084E-5	6.6	-0.08583
6	11.7	2.55166E-5	7	-0.08054
7	12.6	-1.73152E-6	7.4	-0.05559
8	12.9	-1.67194E-5	7.8	-0.07243
9	13.5	-3.9369E-5	8.4	0.50558
10	14.4	-5.43946E-5	9.3	-0.44701
11	14.4	-5.43946E-5	9.7	0.28515
12	15.4	2.92603E-5	10.2	0.18595
13	15.6	-3.05468E-6	10.6	-0.4731
14	15.9	-4.24715E-5	10.9	0.0273
15	16.4	1.2962E-5	11.2	0.13593
16	17.3	4.15847E-5	11.6	0.41824
17	17.5	-1.91974E-5	12.5	-0.80471
18	17.6	-1.25472E-5	13	0.66525
19	17.9	-3.90044E-5	13.9	-0.72156
20	17.9	-3.90044E-5	14.7	0.27817
21	18	-3.43934E-5	15	0.2971
22	18.5	-4.52935E-5	15.2	-0.22274
23	18.5	-4.52935E-5	15.7	-0.43133
24	18.6	1.81624E-5	16.1	0.07363
25	18.9	-3.79437E-5	16.4	0.08212
26	18.9	-3.79437E-5	16.5	-0.07664
27	19	-1.29523E-5	16.7	0.09019
28	19.2	-2.36419E-5	17.2	-0.33251
29	19.3	-4.2118E-5	17.8	0.33712
30	19.3	-4.2118E-5	18.1	0.17749
31	19.8	2.72532E-5	18.4	-0.47448
32	19.9	-3.69108E-5	18.9	-0.55117
33	20	-1.3475E-5	19.7	0.39952

Table 2: Data used in ANNs for model 1 at node 192.

No	Time (s) of Peak Strain	Vertical Peak Strain	Time (s) of Peak Displacement	Vertical Peak Displacement (mm)
1	4.2	-1.3028E-5	0.8	-0.00193
2	8.7	2.55742E-5	1.4	0.039
3	10	-2.30875E-5	2	0.04645
4	11.4	2.36953E-5	2.4	0.012
5	11.9	3.09427E-5	2.5	0.03858
6	12.1	8.26371E-6	2.9	-0.02446
7	12.2	2.12201E-6	3.5	-0.01487
8	12.9	-2.63654E-5	4.1	-0.01416
9	13.3	-2.56894E-5	4.5	0.07741
10	13.7	-3.55372E-5	5.2	-0.10697
11	14.2	2.24323E-5	5.9	0.23836
12	14.5	1.98749E-5	6.4	0.20091
13	14.8	3.11179E-5	7.2	-0.20553
14	15.1	2.28205E-5	8.3	0.23569
15	16.1	-4.67412E-5	9.1	-0.05504
16	16.4	-1.81681E-5	9.7	0.06633
17	16.5	3.34733E-5	10	0.0091
18	16.6	-2.73132E-5	10.2	0.03745
19	16.8	2.01654E-6	10.6	-0.09899
20	17.1	2.96615E-5	11.9	0.34158
21	17.8	-2.63391E-5	12.9	-0.39836
22	18.1	-2.40995E-5	13.8	0.40224
23	18.1	-2.40995E-5	14.4	-0.17259
24	18.2	4.54628E-5	15.1	0.3185
25	18.3	1.11294E-6	16.1	-0.26687
26	18.6	-1.49689E-5	16.8	0.23331
27	18.7	-2.27521E-5	17.1	0.21027
28	19.1	-2.19045E-5	17.3	-0.05233
29	19.2	-1.07561E-6	17.9	0.16137
30	19.3	-4.97683E-5	18.2	0.29323
31	19.4	-9.87762E-6	18.5	0.24324
32	19.6	-3.51647E-5	19.1	-0.2389
33	19.7	3.44068E-5	19.8	0.22637

Table 3: Data used in ANNs for model 2 at node 192.

No	Time (s) of Peak Strain	Vertical Peak Strain	Time (s) of Peak Displacement	Vertical Peak Displacement (mm)
1	11.8	2.07563E-5	1.1	-9.31982E-4
2	11.9	-2.14757E-5	2.2	0.04912
3	12.8	-1.19775E-5	3.2	-0.04446
4	13.7	-8.5937E-8	4	0.04448
5	13.9	-4.18506E-6	4.6	-0.02776
6	14	1.74155E-5	5.4	0.08549
7	14.1	2.52645E-5	6.1	-0.07784
8	14.7	5.44731E-7	6.9	0.1135
9	15	3.02762E-5	7.8	-0.06366
10	15.3	4.2301E-5	8.5	0.14371
11	15.9	-1.88E-5	9.3	-0.07478
12	16.1	1.99012E-5	10.3	0.16302
13	16.4	2.78226E-5	11.3	-0.27656
14	16.8	-2.01119E-5	12.3	0.46863
15	16.9	-1.24433E-5	13.1	-0.34137
16	17	2.35534E-5	13.8	0.35243
17	17.4	-2.04325E-5	14.1	0.24636
18	17.4	-2.04325E-5	14.5	-0.18729
19	17.6	2.17913E-5	14.9	-0.10603
20	17.6	2.17913E-5	15.3	0.40707
21	17.7	-2.68727E-5	15.6	0.40274
22	18	-4.45752E-5	16.3	-0.50955
23	18.1	1.64394E-5	17	0.54821
24	18.4	4.00299E-5	17.9	-0.35257
25	18.7	6.92011E-6	18.4	0.22553
26	18.9	1.47135E-5	18.7	0.27565
27	19	-6.47186E-6	19	0.22177
28	19.2	-6.47131E-6	19.4	-0.0398
29	19.4	-3.17943E-5	19.7	0.07224
30	19.7	-1.95444E-5	19.8	0.00777
31	19.7	-1.95444E-5	1.1	-9.31982E-4
32	19.9	4.86036E-7	2.2	0.04912
33	20	2.75958E-5	3.2	-0.04446

Table 4: Data used in ANNs for model 3 at node 192.

No	Time (s) of Peak Strain	Vertical Peak Strain	Time (s) of Peak Displacement	Vertical Peak Displacement (mm)
1	13.5	3.49656E-5	3.7	-0.02382
2	13.9	4.56664E-5	5.1	0.03901
3	15.1	6.21655E-5	5.4	0.0315
4	15.3	4.32877E-5	6	-0.0352
5	15.5	3.55169E-5	6.8	0.02722
6	15.5	3.55169E-5	7	-0.03207
7	15.6	-3.81852E-5	7.6	-0.03201
8	15.9	5.5054E-5	7.8	0.04521
9	16.1	-3.8902E-5	8.3	0.0512
10	16.2	4.48545E-5	9	-0.02201
11	16.3	-5.66588E-5	9.8	0.02609
12	16.5	7.32731E-5	9.9	-0.02686
13	16.9	-4.22031E-5	10.5	0.05561
14	17	2.61352E-5	10.9	-0.02357
15	17.1	6.98217E-5	11.7	0.06574
16	17.2	6.9958E-5	12.1	0.09113
17	17.3	4.10507E-5	13.1	-0.30422
18	17.3	4.10507E-5	13.5	0.03494
19	17.5	1.67097E-5	13.7	-0.1781
20	17.8	1.21767E-5	13.9	0.5977
21	17.9	4.85343E-5	14.6	0.14167
22	18.1	-8.11604E-5	14.9	-0.3594
23	18.2	8.66784E-5	15.3	0.07141
24	18.4	-5.18286E-5	15.6	-0.12681
25	18.7	-5.93208E-5	15.9	0.37987
26	18.8	4.26183E-5	16.1	-0.26379
27	19.1	2.64145E-5	16.5	0.22709
28	19.2	4.78482E-5	16.7	-0.38467
29	19.4	-6.44013E-5	17.4	0.40609
30	19.4	-6.44013E-5	17.6	-0.1747
31	19.5	-7.55963E-5	18.1	-0.64465
32	19.7	5.7718E-5	18.9	0.39326
33	19.8	-4.45848E-5	19.4	-0.15696

Table 5: Data used in ANNs for model 4 at node 192.
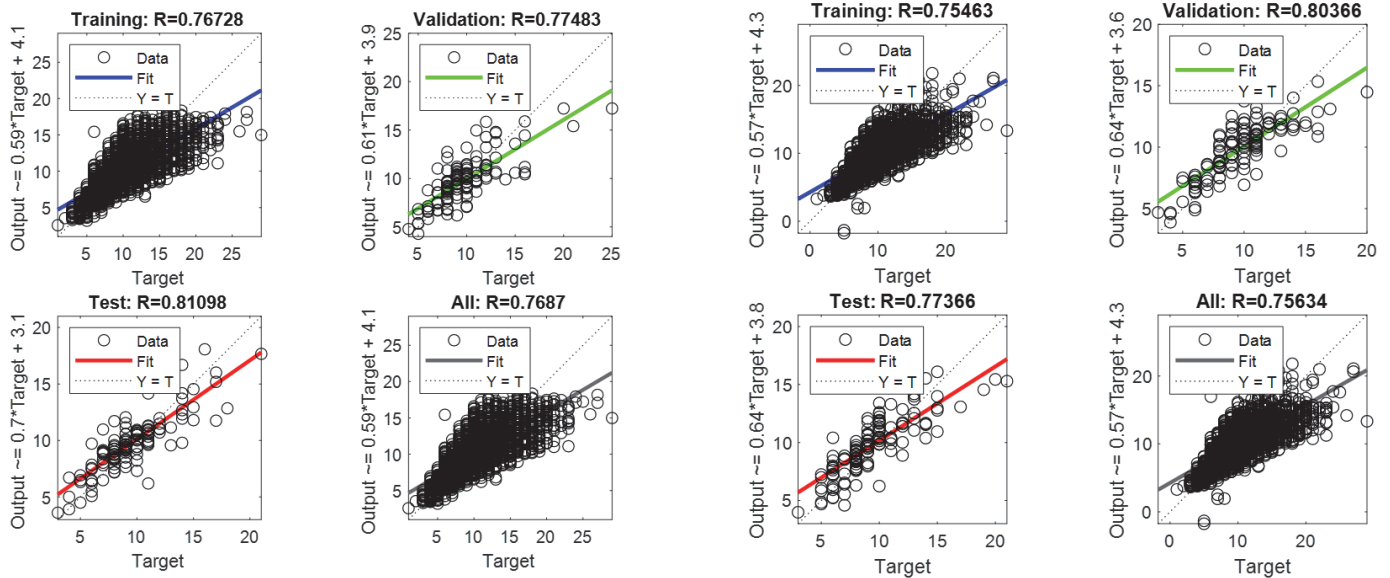
Model - 1, with 24.9 (km) distances to earthquake's epicenter
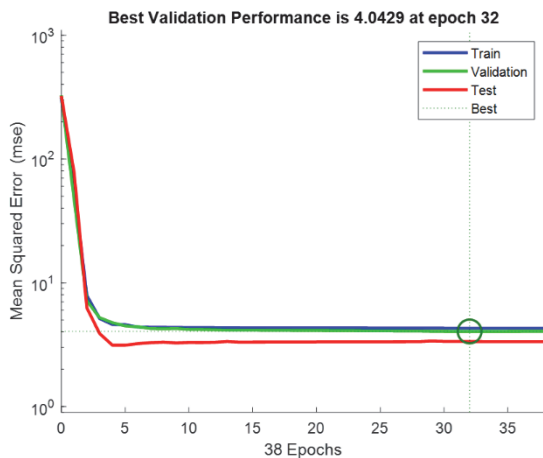
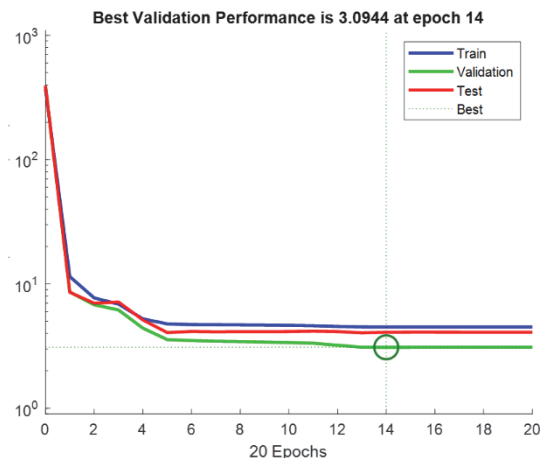Model - 2, with 38.3 (km) distances to earthquake's epicenter
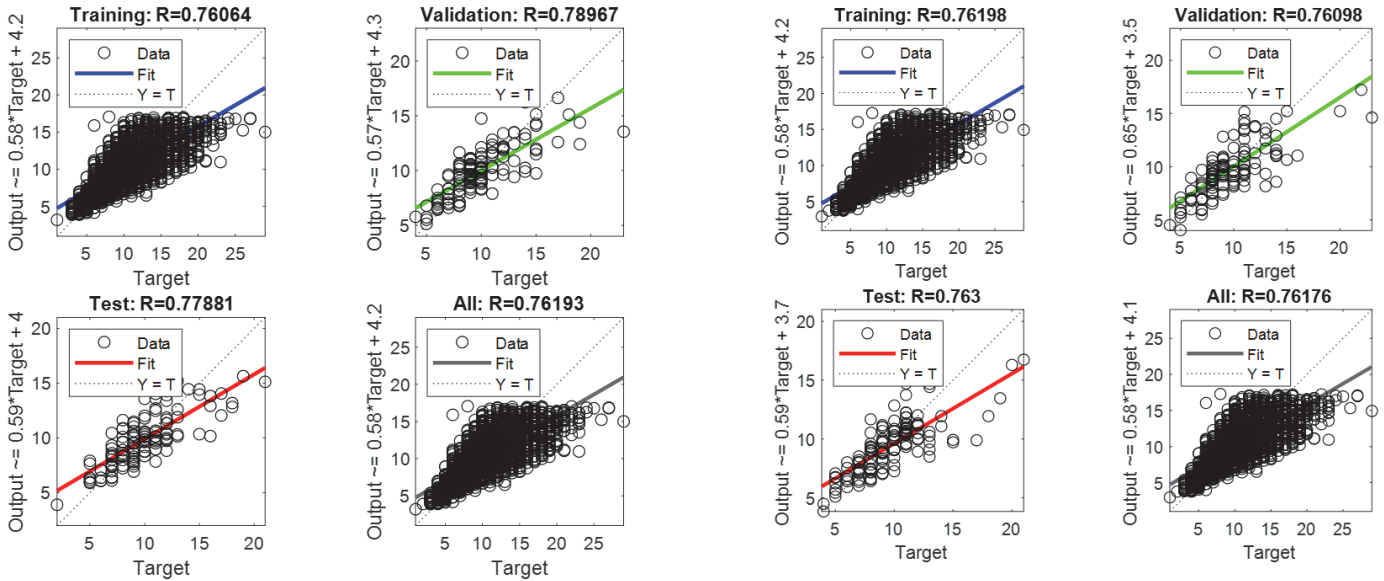
Model - 3, with 65.9 (km) distances to earthquake's epicenter

Model - 4, with 84.5 (km) distances to earthquake's epicenter

Figure 10: Regression analysis for displacement prediction in Y direction in models 1- 4 at node 192.

Model - 1, with 24.9 (km) distances to earthquake's epicenter

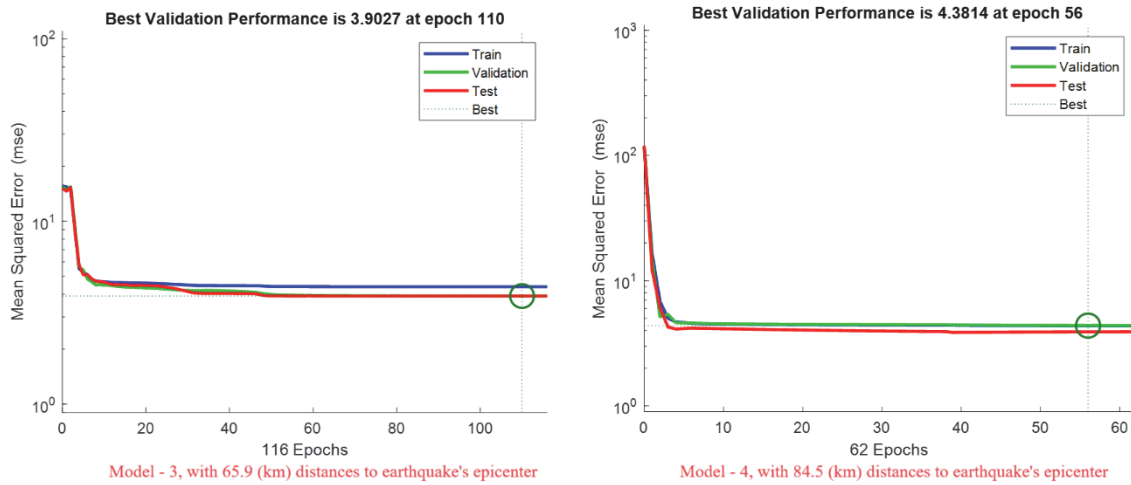Model - 2, with 38.3 (km) distances to earthquake's epicenter

Figure 11: Prediction of displacement in Y direction for models 1-4 at node 192.

	-	Training	Validation	Test	Number of layers in ANNs
Model- 1	R^2	0.76728	0.77483	0.81098	2
	RMSE	4.2872	4.0429	3.353	2
Model- 2	R^2	0.75463	0.80366	0.77366	2
	RMSE	4.5024	3.0944	4.0887	2
Model- 3	R^2	0.76064	0.78967	0.77881	2
	RMSE	4.3886	3.9027	3.8994	2
Model- 4	R^2	0.76198	0.76098	0.763	2
	RMSE	4.3759	4.3814	3.9123	2

Table 6: R^2 and RMSE outcomes of ANNs for models 1-4 at node 192.

CONCLUSION

A nonlinear numerical simulation was conducted to assess the impact of the earthquake's distance on the crack propagation of soil. The numerical modeling of soil categorized as a no-tensile material was adopted to explain the deformation of the crack-growing path simulated using the XFEM. ANN was used to predict maximum displacement in a selected point of each model.

- In the event of an earthquake, the acceleration history (g) characteristics for different distances from the epicenter can vary. The nature of applying seismic load on the model at a different distance from the earthquake's epicenter is different.
- It was observed that the model's failure pattern changes with the earthquake's associated distance. The seismic resistance of the embankment is related to the distance from the epicenter of the earthquake and the soil layers that seismic waves transfer from the earthquake's epicenter to the embankment.
- By increasing the distance of the embankment to the earthquake's epicenter, the time for the occurrence of the maximum negative and positive displacement exhibits nonlinearity. The impact of earthquake-related displacement from the epicenter must be classified based on a specific distance range.
- This study helps to understand the failure mode of the model and introduces a new classification in earthquake damage prediction.
- In practical seismic embankment design, there is a need for the seismic embankment at different distances from the epicenter of an assumed earthquake, and results have to be integrated by applying ANN.

REFERENCES

[1] Vallejo, L.E. (1988). The brittle and ductile behavior of clay samples containing a crack under mixed mode loading. Theor. Appl. Fract. Mech. 10, pp. 73-78. DOI: 10.1016/0167-8442(88)90058-4.

[2] Shimbo, T., Shinzo, Ch., Uchii, U., Itto, R., Fukumoto, Y. (2022). Effect of water contents and initial crack lengths on mechanical properties and failure modes of pre-cracked compacted clay under uniaxial compression. Engineering Geology 301 (2022) 106593. DOI: 10.1016/j.enggeo.2022.106593.

[3] Harison, J.A., Hardin, B.O., Mahboub, K. (1994). Fracture toughness of compacted cohesive soils using ring test. J. Geotech. Eng. 120, pp. 872–891. DOI:10.1061/(ASCE)0733-9410(1994)120:5(872).

[4] Rankine, W. (1857). On the stability of loose earth. Philosophical Transactions of the Royal Society of London, 147.

[5] Namdar, A., Karimpour-Fard, M., Berto, F., Muhammad, N. (2023). Prediction of the displacement mechanism of the cracked soil using NXFEM and Artificial Neural Networks. Procedia Struct. 47, pp. 636-645. DOI: 10.1016/j.prostr.2023.07.058.

[6] Mughieda. O. S., Al-Sharif, M. (2013). Suitability of Irbid Clay as Compacted Liners for Landfill, Jordan. Int. j. geosci. 4, pp. 1509-1512. DOI:10.4236/ijg.2013.410148.

[7] Sun, W., Bao, Sh., Zhou, J., Ni, P. (2023). Concurrent multiscale analysis of anti-seepage structures in embankment dam based on the nonlinear Arlequin method. Eng Anal Bound Elem. 149, pp. 231-247. DOI: 10.1016/j.enganabound.2023.01.039.

[8] Harada, Y., Goto, H., Sawada, S. (2022). Initiation process of tension cracks in soil embankment on liquefied sandy ground investigated from centrifuge model test. Soil Dyn. Earthq. Eng. 161, 107444. DOI:10.1016/j.soildyn.2022.107444.

[9] Namdar, A. Dong, Y. (2020). The embankment-subsoil displacement mechanism, Mater. Des. Process Comm. e155 (2020) 1-4. DOI:10.1002/mdp2.155.

[10] Han, J., Oztoprak, S., Parsons, R.L., Huang, J. (2007). Numerical analysis of foundation columns to support widening of embankments. Comput Geotech. 34, pp. 435–448. DOI: 10.1016/j.compgeo.2007.01.006.

[11] Pham, T. A., Guo, Xi., Dias, D. (2022). Internal stability analysis of column-supported embankments: Deterministic and probabilistic approaches. Transportation Geotechnics 37, 100868. DOI: 10.1016/j.trgeo.2022.100868.

[12] Namdar, A., Berto, F. (2022). The improvement embankment seismic resistance by selecting suitable geogrid locations in the subsoil. Procedia Struct. 41, pp. 403-411. DOI:10.1016/j.prostr.2022.05.046.

[13] Namdar, A. (2022). Impact of soil crack on embankment seismic resistance. Procedia Struct. 39, pp. 47-56. DOI:10.1016/j.prostr.2022.03.071.

[14] Sakai, T., Inukai, Sh., Inagaki, M., Nakano, M. (2023). Improvement in seismic resistance using replacement/counterweight fill method for existing high embankments on inclined ground constructed with various embankment materials. Soils Found. 63, 101284. DOI: 10.1016/j.sandf.2023.101284.

[15] Tay, YY., Stewart, DI., Cousens, TW. (2001). Shrinkage and desiccation cracking in bentonite-sand landfill liners. Eng Geol. 60, pp. 263–74. DOI:10.1016/S0013- 7952(00)00107-1.

[16] Savage, S., Douglas, K., Fell, R., Peirson, W. (2019). Modeling the erosion and swelling of the sides of transverse cracks in embankment dams. J Geotech Geoenviron Eng. 145(5), 04019015. DOI:10.1061/(ASCE)GT.1943-5606.0002040.

[17] Liu, W., Yu, W., Hu, D., Lu, Y., Chen, L., Yi, Xi., Han, F. (2019). Crack damage investigation of paved highway embankment in the Tibetan Plateau permafrost environments. Cold Reg. Sci. Technol. 163, pp. 78–86. DOI:10.1016/j.coldregions.2019.05.003.

[18] Wu, Z.W., Liu, Y.Z. (2005). Frozen Subsoil and Engineering, Ocean Press, Beijing.

[19] Maharjan M, Takahashi A. (2014). Liquefaction-induced deformation of earthen embankments on non-homogeneous soil deposits under sequential ground motions. Soil Dynam Earthq Eng 66, pp. 113–24. DOI:10.1016/j. soildyn.2014.06.024.

[20] Bui, H., Tandrijana, V., Fell, R., Song, C., Khalili, N. (2005). Two and three dimensional numerical modelling of the potential for cracking of embankment dams -supplementary report. UNICIV Report No. R-438, School of Civil and Environmental Engineering, University of New South Wales, Sydney, Australia.

[21] He, K., Fell, R., Song, C. (2019). Transverse cracking in embankment dams resulting from cross-valley differential settlements. Eur. J. Environ. Civil Eng. pp. 1–27. DOI:10.1080/19648189.2019.1691663.

[22] Okamura M, Tamamura S, Yamamoto R. (2013). Seismic stability of embankments subjected to pre-deformation due to foundation consolidation. Soils Found 53 (1), pp. 11–22. DOI:10.1016/j.sandf.2012.07.015.

[23] Ling JM, Qian JS, Huang QL. (2003). New technologies of subgrade widening for highways. Internal Report, Tongji University and Changsha Science and Technology University [in Chinese].

[24] Namdar, A., Karimpour-Fard, M., Muhammad, N. (2022). The seismic resistance simulation for cracked clayey backfill. Eng. Fail. Anal. 140, 106616. DOI: 10.1016/j.engfailanal.2022.106616.

[25] Namdar, A., Berto, F., Muhammad, N. (2022). The displacement simulation for cracked earth structure with different geometry. Procedia Struct. 41, pp. 394-402. DOI:10.1016/j.prostr.2022.05.045.

[26] Li, K., Xu, W., Yang, L. (2021). Deformation Characteristics of Raising, Widening of Old Roadway on Soft Soil Foundation. Symmetry. 13(11), 2117. DOI:10.3390/sym13112117.

[27] Yasuda, S. (2023). Seismic inspection and countermeasures for existing embankments in Japan. Soil Dyn. Earthq. Eng. 172, 108004. DOI: 10.1016/j.soildyn.2023.108004.

[28] Yamaguchi, Y., Kondo, M., Kobori, T. (2012). Safety inspections and seismic behavior of embankment dams during the 2011 off the Pacific Coast of Tohoku earthquake. Soils Found. 52(5), pp. 945–955.
DOI: 10.1016/j.sandf.2012.11.013.

[29] Tian, Y., Yang, Zh., Liu, Y., Cai, Xi., Shen, Y. (2021). Long-term thermal stability and settlement of heat pipe-protected highway embankment in warm permafrost regions. Eng. Geol. 292, 106269. DOI:10.1016/j.enggeo.2021.106269.

[30] Yamaguchi, Y., Iwashita, T., Mitsuishi, S. (2008). Preliminary investigation of dams stricken by the Iwate-Miyagi Nairiku Earthquake in 2008, In: Proceedings of the 5th EADC International Symposium on Co-existence of Environment and Dams.

[31] He, K., Song, Ch., Fell, R. (2021). Numerical modelling of transverse cracking in embankment dams. Comput. Geotech. 132, 104028. DOI: 10.1016/j.compgeo.2021.104028.

[32] Boulanger, R.W., Khosravi, M., Khosravi, A., Wilson, D.W. (2018). Remediation of liquefaction effects for an embankment using soil-cement walls: Centrifuge and numerical modeling. Soil Dyn. Earthq. Eng. 114, pp. 38-50. DOI:10.1016/j.soildyn.2018.07.001.

[33] Guo, L., Li, W., Namdar, A. (2021). Using recycled aggregate for seismically monitoring of embankment-subsoil model. Case Stud. Constr. Mater. 15 (3) e00605. DOI:10.1016/j.cscm.2021.e00605.

[34] Jamshidi Chenari, R., Bathurst, R.J. (2023). Influence of geosynthetic stiffness on bearing capacity of strip footings seated on thin reinforced granular layers over undrained soft clay. Geotext. Geomembr. 51, pp. 43-55.
DOI: 10.1016/j.geotexmem.2022.09.006.

[35] Wu, J., El Naggar, M. H., Li, Xi., Wen, H. (2020). DEM analysis of geobag wall system filled with recycled concrete aggregate, Constr. Build. Mater. 238, 117684. DOI:10.1016/j.conbuildmat.2019.117684.

[36] Li, Y., Cai, W., Zhu, W., Dong, Z., Zhang, Q. (2019). Particle flow analysis of parallel double crack evolution under uniaxial compression. J. Cent. South Univ. Sci. Technol. 50, pp. 3035-3045.
DOI: 10.11817/j.issn.1672-7207.2019.12.013.

[37] Rowe, R.K., Quigley, R.M., Booker, J.R. (1995). Clayey Barrier Systems for Waste Disposal Facilities, E & FN Spon, London, p. 390.

[38] Center for Engineering Strong Motion Data (CESMD), https://strongmotioncenter.org/

[39] Namdar, A. (2021). The boundary condition simulation quality for embankment seismic response. Eng. Fail. Anal. 126, 1054a91. DOI: 10.1016/j.engfailanal.2021.105491.

[40] Craig, R.F. (2004). Soil Mechanics. Spon Press. Taylor & Francis Group.

[41] Potts, D. M., Zdravkovik, L. (1999). Finite element analysis in geotechnical engineering theory. Thomas Telford Publishing, Thomas Telford Ltd, 1 Heron Quay, London E14 4JD.

[42] Nyaoro, D.L. (1989). Analysis of soil-structure interaction by finite elements. PhD thesis, Imperial College, University of London.

[43] Belytschko, T., Black. T. (1999). Elastic crack growth in finite elements with minimal remeshing. Internat. J. Numer. Methods Engrg. 45, pp. 601-620. DOI: 10.1002/(SICI)1097-0207(19990620)45:53.0.CO;2-S.

[44] Moes, N., Dolbow, J., Belytschko, T. (1999). A finite element method for crack growth without remeshing. Internat. J. Numer. Methods Engrg. 46, pp. 131-150.

[45] Hansbo, A., Hansbo, P. A. (2004). Finite element method for the simulation of strong and weak discontinuities in solid mechanics. Comput Methods Appl Mech Eng. 193, 3523-3540. DOI:10.1016/j.cma.2003.12.041.

[46] Lua, J., Zhang, T., Fang, E., Song, J.H. (2016). Explicit phantom paired shell element approach for crack branching and impact damage prediction of aluminum structures. International Journal of Impact Engineering 87, pp. 28–43. DOI:10.1016/j.ijimpeng.2015.07.007.

[47] Namdar, A. (2020). The application of soil mixture in concrete footing design using linear regression analysis. Mater. Des. Process Comm., e179. DOI:10.1002/mdp2.179.

[48] Namdar, A. (2021). Design geometry of the embankment for minimize nonlinear displacement. Mater. Des. Process Comm. e209. DOI: 10.1002/mdp2.209.

[49] Namdar, A. (2020). Forecasting bearing capacity of the mixed soil using artificial neural networking. Frat. ed Integrita Strutt. 14 (53), pp. 285-294. DOI:10.3221/IGF-ESIS.23.22.

[50] Omar, M., Shanableh, A., Mughieda, O., Arab, M., Zeiada, W., Al-Ruzouq, R. (2018). Advanced mathematical models and their comparison to predict compaction properties of fine-grained soils from various physical properties. Soils Found. 58, pp. 1383-1399. DOI:10.1016/j.sandf.2018.08.004.

[51] Mughieda, O. S., Bani-Hani, Kh., Abu Safieh, B.F. (2009). Liquefaction assessment by artificial neural networks based on CPT. J. Geotech. Eng 3: 289-302. DOI:10.3328/IJGE.2009.03.02.289-302.

[52] Namdar, A., Karimpour-Fard, M., Mughieda, O., Berto, F., Muhammad, N. (2023). Crack simulation for the cover of the landfill – A seismic design. Frat. ed Integrita Strutt 65, pp. 112-134. DOI:10.3221/IGF-ESIS.65.09.

[53] Alperen Soyer, M., Tüzün, N., Karakaş, Ö., Berto, F. (2023). An investigation of artificial neural network structure and its effects on the estimation of the low-cycle fatigue parameters of various steels. FFEMS. pp. 2929-2948. DOI:10.1111/ffe.14054.

[54] Sreekanth, T. G. ., Senthilkumar, M. and Reddy, S. M. (2022). Natural Frequency based delamination estimation in GFRP beams using RSM and ANN. Frat. ed Integrita Strutt. 16(61), pp. 487–495. DOI: 10.3221/IGF-ESIS.61.32.

[55] Ouladbrahim, A., Belaidi, I., Khatir, S., Magagnini, E., Capozucca, R., Abdel Wahab, M. (2021). Sensitivity analysis of the GTN damage parameters at different temperature for dynamic fracture propagation in X70 pipeline steel using neural network. Frat. ed Integrita Strutt, 15(58), pp. 442-452. DOI:10.3221/IGF-ESIS.58.32.

[56] Bui-Tien, T., Bui-Ngoc, D., Nguyen-Tran, H., Nguyen-Ngoc, L., Tran-Ngoc, H. and Tran-Viet, H. (2021). Damage Detection in Structural Health Monitoring using Hybrid Convolution Neural Network and Recurrent Neural Network. Frat. ed Integrita Strutt. 16(59), pp. 461–470. DOI: 10.3221/IGF-ESIS.59.30.

[57] Sreekanth, T. G., Senthilkumar, M., Manikanta Reddy, S. (2022). Artificial neural network based delamination prediction in composite plates using vibration signals. Frat. ed Integrita Strutt. 17(63), pp. 37-45. DOI: 10.3221/IGF-ESIS.63.04.

[58] Ahmadi, F., Rahbar Ranji, A., Nowruzi, H. (2020). Ultimate strength prediction of corroded plates with center-longitudinal crack using FEM and ANN. Ocean Eng. 206, 107281. DOI: 10.1016/j.oceaneng.2020.107281.

[59] Trevor, H., Robert, T., Jerome, F. (2009). The Elements of Statistical Learning: Data Mining, Inference, and Prediction. Springer, New York, NY.

[60] Li, D., Chen, Zh., Li, J., Yi, J. (2022). Ultimate strength assessment of ship hull plate with multiple cracks under axial compression using artificial neural networks. Ocean Eng. 263, 112438. DOI: 10.1016/j.oceaneng.2022.112438.

[61] Devore, J., Farnum, N., Doi, J. (2014). Applied Statistics for Engineers and Scientists. Publisher Richard Stratton.

[62] Soyer, MA., Tüzün, N., Karakaₛs, Ö., Berto, F. (2023). An investigation of artificial neural network structure and its effects on the estimation of the low-cycle fatigue parameters of various steels. Fatigue Fract Eng Mater Struct. 46(8), pp. 2929-2948. DOI:10.1111/ffe.14054.

[63] Stone, M. (1974). Cross-validatory choice and assessment of statistical predictions. J. Roy. Stat. Soc. B. 36, 111-147.

[64] Shahin, M.A., Maier, H.R., Jaksa, M.B. (2002). Predicting settlement of shallow foundations using neural network. J. Geotech. Geoenviron. Eng. ASCE. 128 (9), pp. 785-793.

[65] Shanmuganathan, S., Samarasinghe, S. (2016). Artificial Neural Network Modelling. 628. Cham, Switzerland: Springer, 2016.

[66] Haykin, S. S. (2009). Neural networks and learning machines. 3, Pearson Upper Saddle River, NJ, USA.

[67] Priddy, K.L., Keller, P.E. (2005). Artificial neural networks: an introduction. 68, SPIE press.